Amplification of Single Mechanical Fault Signatures Using Full Adaptive PMSM Observer

Mohamed Lamine Masmoudi, Erik Etien, Sandrine Moreau, and Anas Sakout

Abstract—This paper presents a localized mechanical fault detection method using a full adaptive permanent-magnet synchronous machine (PMSM) observer in a *d/q* reference frame. It appears that the fault sensitivity of PMSM stator currents and rotor speed measurements is very low with regard to single mechanical faults. That is why an amplification of single mechanical fault signatures in frequency domain is proposed by adjusting the adaptive PMSM observer gains. To study the influence of the adaptive PMSM observer gains on fault signatures, the observer model is first of all linearized at an operating point. Then, the static gain, the resonance, and the quality factor *Q* of different transfer functions are analyzed. A dedicated experimental setup based on an original mechanical fault emulator and a 7.8 kW PMSM drive is designed to validate the simulation results. The simulation and the experimental results show that the proposed method is effective to amplify single mechanical fault signatures and the calculated fault indicator.

Index Terms—Adaptive observer design, fault diagnosis, permanent-magnet synchronous machine (PMSM), signature amplification, single mechanical fault.

I. INTRODUCTION

THE state-of-the-art in research into condition monitoring and fault diagnosis shows that electrical machines are complex electromechanical systems which often work under very rough conditions. Thus, they are subjected to multiple failures which may occur in the stator, in the rotor, in the bearings, or in the gearbox. Mechanical faults represent two-thirds of motor failures [1]. This kind of failure is generally supervised through different strategies, such as vibration, temperature, or oil monitoring, etc. [2]–[4]. In these techniques, extra sensors are installed in order to provide signals to be analyzed with various signal processing methods. Another way is to consider the motor as a sensor. In this case, different signals as currents, voltages, speed, torque, or magnetic flux can be used to perform the monitoring. Among these methods, motor current signature analysis (MCSA) presents several benefits since it is an inexpensive and noninvasive technique [5]–[8].

Monitoring amplitude and frequency of the current signals, fault signatures could be tracked easily. It is well established that the frequency is the signal containing the more information about the fault. Several methods were elaborated based on fast Fourier transform, Wavelets, Hilbert transform, Park's vector approach or advanced methods based on artificial intelligence techniques in order to extract those faults. A general review of the different methods based on MCSA is presented in [9]–[12].

In the case of localized faults, the faults components are produced at predictable sidebands frequencies related to the current frequency. Under low deterioration (small fault), their detection is not always guaranteed, because of the fault components low amplitude in the current signal [13]. To overcome this problem, an amplification procedure is needed to amplify and extract those small fault signatures. In the case of synchronous motors, the current frequency analysis is similar to the rotation speed analysis. Hence, faults can be tracked using a direct speed measurement or observers [15]–[18].

Another way to estimate the rotation speed in the case of synchronous machine is to calculate the PLL which is defined as the instantaneous frequency. However, it represents several downsides specially with induction machine speed estimation which is the major flaw. It is characterized also by its narrow lock range and its capture range that depend on the voltage-controlled oscillation and the loop filter design which is a challenge when the rotation speed is highly variable. On the other hand, rotation speed estimation using an observer rises above the PLL limitations, estimates rotation speed without extra sensors, and amplifies specific frequencies on the estimated signal in order to overcome the problem cited before.

This paper presents a localized fault diagnosis using an adaptive observer in the $\{d/q\}$ frame. A particular design is performed to highlight signatures in the motor mechanical speed in order to overcome the low fault signatures amplitude in the case of low degradation. Tests are carried out on an original test bench which was designed to simulate localized faults, such as gears and bearings faults. In Section II, mechanical fault characteristic frequencies expressions are defined. In Section III, the permanent-magnet synchronous machine (PMSM) observer model is defined. Then the fault signatures amplification feature of the PMSM observer is studied. In Section V, the original localized faults emulator is presented. The experimental data validate the single fault diagnosis procedure using a high-resolution technique to estimate the fault frequency and the defined fault indicator *R* in order to discriminate faulty cases.

M. L. Masmoudi, E. Etien, and S. Moreau are with the Laboratoire d'Informatique et d'Automatique pour les Systémes, University of Poitiers, 86000 Poitiers, France (e-mail: ml_masmoudi@yahoo.com; erik.etien@univ-poitiers.fr; sandrine.moreau@univ-poitiers.fr).

A. Sakout is with the LaSIE laboratory, University of La Rochelle, 17000 La Rochelle, France (e-mail: asakout@univ-lr.fr).

II. FAULT SIGNATURES ON THE ROTATION SPEED

Single or localized faults are generally referred to single bearing faults or tooth fault in gearboxes. This kind of failure generates an abnormal load affecting the machine torque. The load torque can be modeled as a constant component Γ_0 and a fault component varying at the characteristic frequency f_d

$$\Gamma_{\text{load}}(t) = \Gamma_0 + \delta_\Gamma(t). \tag{1}$$

In this paper, the additional torque $\delta_\Gamma(t)$ is modeled as a periodic impulse signal with a periodicity related to the mechanical position (θ_m). The disturbance torque $\delta_\Gamma(t)$ is written using its Fourier series as

$$\Gamma_{\text{load}}(t) = A \times D \left[1 + 2\sum_{n=1}^{\infty}\left(\frac{\sin(n\pi R)}{n\pi R}\right)\right]\cos(n\theta_d) \tag{2}$$

where A is the amplitude of the fault-related torque, R is the duty cycle defined by $D = \frac{\varepsilon}{T_o}$ with ε the pulse width, and T_o is the related signal periodicity. The angle θ_d is related to the mechanical position θ_m by

$$\theta_d = N_i\theta_m. \tag{3}$$

The parameter N_i permits to choose the number of impacts for one rotor revolution. At constant speed, the relationship between the fundamental default frequency (f_d) and the mechanical frequency (f_m) is

$$f_d = N_i f_m. \tag{4}$$

The following mechanical equation traduces the transfer of torque variations to the rotation speed signal:

$$w_m(t) = \frac{1}{J_m}\int_{t_0}^{t}(\Gamma_{\text{motor}}(\tau) - \Gamma_{\text{load}}(\tau))d\tau \tag{5}$$

with J_m, the total inertia of the system.

Considering that the integration is a linear operation, then the rotational speed contains harmonic components at the same frequencies as (2). It can be used as an effective signal to perform fault detection. However, harmonic amplitudes can be small and difficult to detect. Results depend on mechanical characteristics, in particular of the total inertia J_m. Then, it is interesting to use a speed signal where fault frequencies can be amplified. Here, this goal is achieved by the use of an observer with an appropriate design.

III. PSSM OBSERVER

A. PMSM Model

The stator voltage equation of sinusoidal PMSM in Park's $\{d/q\}$ reference frame fixed to the rotor is modeled as [14]

$$u_s = R_s i_s + \dot{\psi}_s + \omega J\psi_s \tag{6}$$

where $u_s = [u_d \ u_q]^T$ is the stator voltage, $i_s = [i_d \ i_q]^T$ is the stator current, $\psi_s = [\psi_d \ \psi_q]^T$ is the stator flux, R_s is the stator resistance, $\omega = \dot{\theta}$ is the electrical angular speed of the rotor, and
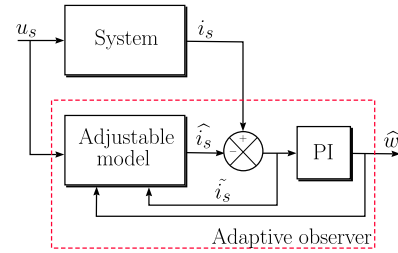

Fig. 1. Block diagram of the system and the adaptive observer.

J is a square matrix represented as

$$J = \begin{bmatrix} 0 & -1 \\ 1 & 0 \end{bmatrix}.$$

The stator flux is written as

$$\psi_s = Li_s + \psi_{\text{pm}} \tag{7}$$

where ψ_{pm} is the permanent magnet flux expressed as $\psi_{\text{pm}} = [\psi_{\text{pm}} \ 0]^T$ and L is the inductance matrix which depends respectively on the direct and quadrature axis inductances L_d and L_q

$$L = \begin{bmatrix} L_d & 0 \\ 0 & L_q \end{bmatrix}.$$

The electromagnetic torque is given by

$$T_e = \frac{3}{2}p\psi_s^T J^T i_s \tag{8}$$

where p is the number of pole pairs.

B. Adaptive Observer

The rotor speed and position estimation in adaptive observers is based on the error estimation between the measured stator currents and the estimated ones. Then, an adaptation mechanism is constructed using the stator currents error estimation in order to estimate the rotor speed. The adjustable model is fed back by the output of the adaptation mechanism, i.e., the rotor speed in the present case.

The adaptive observer scheme is represented in Fig. 1, where stator currents are chosen as state variables in the adjustable model.

Based on (6) and (7), the adaptive observer model can be written as [14], [19]

$$\dot{\widehat{\psi}}_s = u_s - R_s\widehat{i}_s - \widehat{\omega}J\widehat{\psi}_s + \lambda\tilde{i}_s \tag{9}$$

where the superscript $\widehat{\ }$ denotes the estimated quantities. The stator currents estimation and its error are respectively defined as

$$\widehat{i}_s = L^{-1}\left(\widehat{\psi}_s - \psi_{\text{pm}}\right) \tag{10}$$

$$\tilde{i}_s = i_s - \widehat{i}_s. \tag{11}$$

λ is the feedback gain matrix. In order to place two poles of the observer in the complex plane at a specific location, λ should include a symmetric part and skew symmetric part as it

is expressed in (12), where I represents the two-by-two identity matrix and λ_1, λ_2 are scalar gain parameters

$$\lambda = \lambda_1 I + \lambda_2 J. \tag{12}$$

There are several alternative ways to calculate the currents error. In the following, the error is calculated as

$$\epsilon = \begin{bmatrix} 0 & L_q \end{bmatrix} \cdot \tilde{i}_s. \tag{13}$$

To estimate the electrical angular speed of the rotor, an adaptation mechanism based on proportional–integral (PI) regulator is used

$$\widehat{\omega} = -k_p \cdot \epsilon - k_i \int \epsilon \cdot \mathrm{dt} \tag{14}$$

where k_p and k_i are coefficients of the PI regulator. The rotor position $\widehat{\theta}$ is obtained by integrating the rotor angular speed.

C. Linearization of the Adaptive Observer

A linearization at an operating point of the observer model (9) is performed using the adaptation law (14) as an additional state. According to the system linearization method mentioned in [21], the state vector x can be written as

$$x = x_0 + \delta x \tag{15}$$

where $x_0 = [id_0 \ iq_0 \ w_0]$ and $\delta x = [\delta id \ \delta iq \ \delta w]$. Expressing the resulting system in a component form, the linearized model is defined as

$$\frac{d}{\mathrm{dt}} \begin{bmatrix} \delta \widehat{id} \\ \delta \widehat{iq} \\ \delta \widehat{w} \end{bmatrix} = [A] \begin{bmatrix} \delta \widehat{id} \\ \delta \widehat{iq} \\ \delta \widehat{w} \end{bmatrix} + [B] \begin{bmatrix} \delta vd \\ \delta vq \\ \delta id \\ \delta iq \\ \delta w \end{bmatrix} \tag{16}$$

$$y = [C] \begin{bmatrix} \delta \widehat{id} \\ \delta \widehat{iq} \\ \delta \widehat{w} \end{bmatrix} \tag{17}$$

where

$$A = \begin{bmatrix} \dfrac{-R_s}{L_d} - \lambda_1 & \dfrac{L_q}{L_d} w_0 + \lambda_2 & \dfrac{L_q}{L_d} iq_0 \\ \dfrac{-L_d}{L_q} w_0 - \lambda_2 & \dfrac{-R_s}{L_q} - \lambda_1 & \dfrac{\psi_{pm}}{L_q} - \dfrac{L_d}{L_q} id_0 \\ -a_1 & -a_2 & -a_3 \end{bmatrix}$$

$$B = \begin{bmatrix} \dfrac{1}{L_d} & 0 & \lambda_1 & -\lambda_2 & 0 \\ 0 & \dfrac{1}{L_q} & \lambda_2 & \lambda_1 & 0 \\ 0 & 0 & a_1 & a_2 & a_3 \end{bmatrix}$$

$$C = \begin{bmatrix} 1 & 0 & 0 \\ 0 & 1 & 0 \\ 0 & 0 & 1 \end{bmatrix}.$$

The subscript o stands for the operating point quantities. Parameters a_1, a_2, and a_3 are given in Appendix B.

Noting that the stator currents and the angular speed have become inputs of the new system. These variables contain the original information of the fault. The estimated currents and the
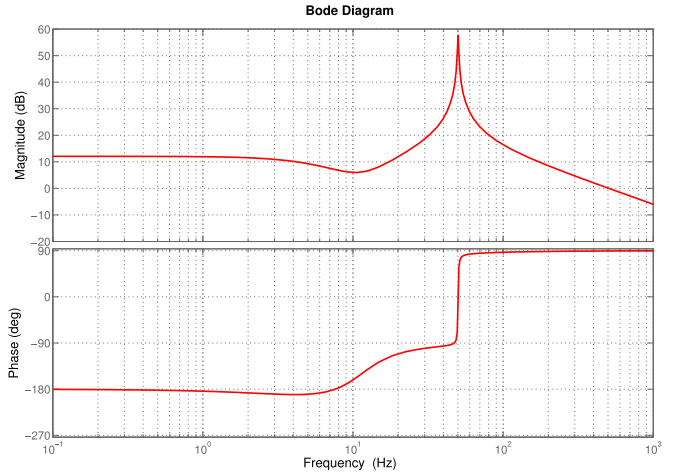

Fig. 2. Bode diagram of the function $F_{34}(s)$ for $\lambda_1 = 15$, $\lambda_2 = 0$, $k_i = 100$ and $k_p = -0.05$.

speed are the outputs. Thus, the observer can be considered as a filter whose parameters will be chosen to amplify the appropriate frequency band for fault detection. Hence, the transfer function between the measured and estimated variables is given by

$$F = C(sI - A)^{-1} B = \begin{bmatrix} F_{11} & F_{12} & \cdots & F_{15} \\ F_{21} & F_{21} & \cdots & F_{25} \\ F_{31} & F_{32} & \cdots & F_{35} \end{bmatrix}. \tag{18}$$

In the following, the transfer function $F_{34}(s) = \dfrac{\widehat{w}(s)}{iq(s)}$ is particularly studied.

IV. ESTIMATED SPEED STUDY

A. Transfer Function Analysis

The transfer function between the stator current iq and the estimated speed $\widehat{w}$ is written as

$$F_{34}(s) = \frac{\widehat{w}(s)}{i_q(s)} = \frac{a_{34.2} s^2 + a_{34.1} s + a_{34.0}}{b_3 s^3 + b_2 s^2 + b_1 s + b_0}. \tag{19}$$

Parameters $a_{34.2}$, $a_{34.1}$, $a_{34.0}$, b_3, b_2, b_1, and b_0 are given in Appendix B. The chosen operating point corresponds to 20% of the nominal rotation speed. With a constant speed w_0, the current iq_0 will be constant. Under the assumption that the parameters of the machine L_d, L_q, and ψ_{pm} are well known, the transfer function $F_{34}(s)$ can be written in function of the parameters k_i, k_p, λ_1, and λ_2. To simplify this transfer function, λ_2 is fixed to 0 as it is proposed in [20]. Thus, the resulting transfer function can be written as a filter where k_i, k_p, and λ_1 are setting parameters.

The chosen operating point corresponds to $w_0 = 62.83$ rad/s, $id_0 = 0$ A, and $iq_0 = 1.78$ A. The Bode diagram of the function $F_{34}(s)$ is given in Fig. 2 for $\lambda_1 = 15$, $\lambda_2 = 0$, $k_i = 100$, and $k_p = -0.05$. According to this figure, we can see that the frequency response of the function $F_{34}(s)$ corresponds to a low-pass filter with a resonance frequency (here at 50 Hz). This resonance frequency can be used for fault detection to amplify the fault signatures in frequency domain by adjusting the three
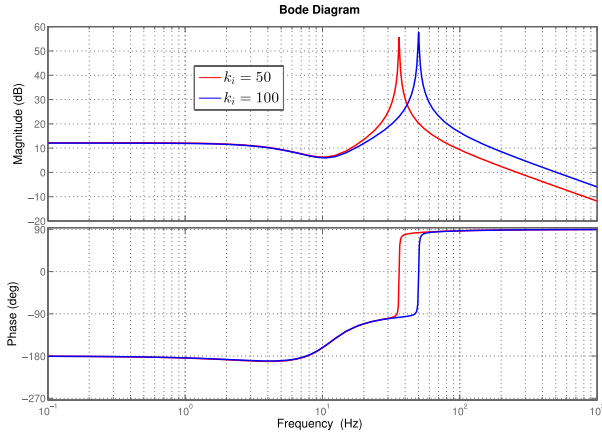
Fig. 3. Bode diagram of the function $F_{34}(s)$ for $\lambda_1 = 15$ and $k_p = -0.05$.
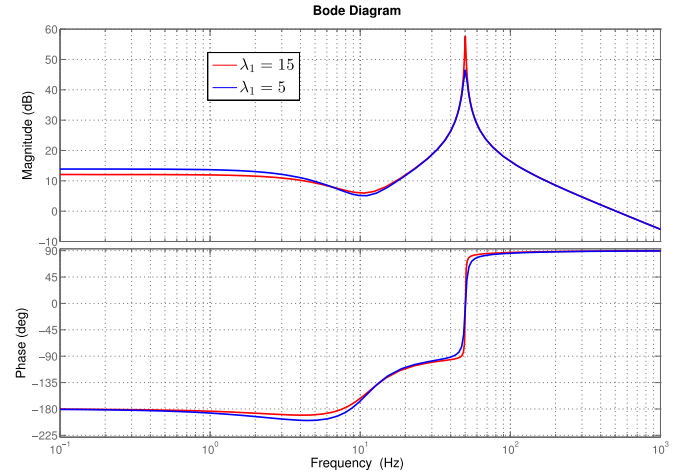

Fig. 4. Bode diagram of the function $F_{34}(s)$ for $\lambda_1 = 15$ and $k_i = 100$.

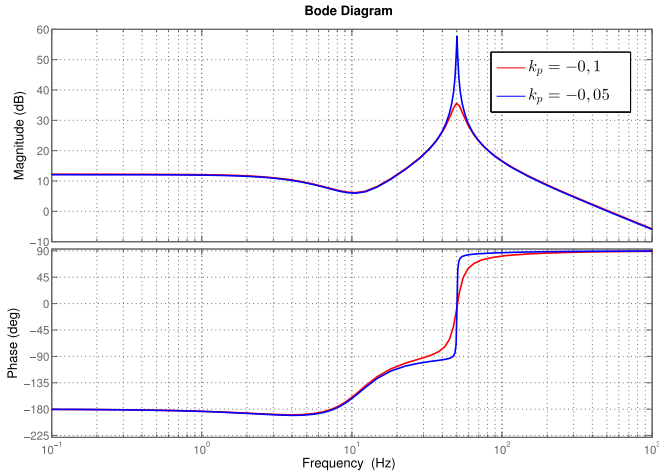Fig. 5. Bode diagram of the function $F_{34}(s)$ for $k_i = 100$ and $k_p = -0.05$.

TABLE I
INFLUENCE OF THE PARAMETERS k_i, k_p, AND λ_1 ON THE TRANSFER
FUNCTION $F_{34}(s)$

	Gain	Resonance Frequency	Q factor
k_i	✓	✓	
k_p	✓		✓
λ_1			✓

$F_{34}(s)$. It means that the observer is reacting as a low-pass filter with a resonance frequency.

B. Observer Design

In the previous section, it was demonstrated that amplifying a specified frequency band with a suitable choice of the observer gains is possible. However, the observer gains setting cannot be performed by taking into account this only criterion since the observer convergence also has to be ensured.

From the state matrix A defined as

$$A = \begin{bmatrix} \dfrac{-R_s}{L_d} - \lambda_1 & \dfrac{L_q}{L_d}w_0 + \lambda_2 & \dfrac{L_q}{L_d}iq_0 \\ \dfrac{-L_d}{L_q}w_0 - \lambda_2 & \dfrac{-R_s}{L_q} - \lambda_1 & \dfrac{\psi_{pm}}{L_q} - \dfrac{L_d}{L_q}id_0 \\ -a_1 & -a_2 & -a_3 \end{bmatrix}$$

it can be noticed that feedback gains λ_1 and λ_2 affect the currents observation dynamics, while k_p and k_i affect the speed dynamics. From Table I, it was seen that on one hand, λ_1 has an effect only on the Q factor and on the other hand, k_p has an effect on both the static gain and the Q factor. In addition, the filter resonance frequency can only be adjusted by the gain k_i. So, the following strategy can be proposed for the observer synthesis.

1) The parameter λ_1 is adjusted to obtain the observer desired dynamics.
2) The parameter k_i is chosen to coincide with a fault frequency.

parameters k_i, k_p, and λ_1 to make the fault frequency coincide with the resonance frequency.

In order to study the influence of those three parameters, the Bode diagram of the function $F_{34}(s)$ is plotted in three different cases. In each case, two parameters are kept constant and the third one varies. Figs. 3, 4, and 5 show the obtained results.

In Fig. 3, it can be noted that the parameter k_i affects the resonance frequency and the static gain of the filter. For $k_i = 50$, the resonance frequency corresponds to 36 Hz and for $k_i = 100$, the resonance frequency increases to 50 Hz. Referring to Fig. 4, the parameter k_p influences both the static gain and the Q factor (quality factor or the damping coefficient) of the filter. For $k_p > 1$, the resonance disappears. Fig. 5 shows the influence of λ_1. It can be noted that increasing this parameter reduces the filter damping without modifying the static gain.

Table I resumes the different parameters interactions with the static gain and Q factor. It should be noticed that k_i is the only parameter which can modify the resonance frequency of the filter.

Note: The influence of the parameters k_i, k_p, and λ_1 on the components $F_{ij}(s)$ ($i = 1, 2, 3$ and $j = 3, 4, 5$) are the same as

Fig. 6. Current open-loop, current closed-loop, and observer poles for $\lambda_1 = 5$.

Fig. 7. Evolution of the sum G in function of the two parameters k_i and k_p.

3) The parameter k_p can be chosen in two ways:

a) To get an acceptable speed dynamics (hence the Q factor will be imposed).

b) To get an optimal amplification of the fault frequencies. In this case, the speed dynamics will be imposed.

In this paper, the second solution is chosen to adjust k_p. Indeed, as the operation speed is constant, the dynamics issue is considered as less crucial.

1) Parameter λ_1: A judicious choice of λ_1 gives to the observer a fast dynamics compared to the current loop one. After having determined the roots of the characteristic equation of the observer model (6) defined by $\det[sI - (A - \lambda C)] = 0$, Fig. 6 shows in the $\Re/Im$ plane the observer poles and the PMSM poles in open and current closed loop respectively for $\lambda_1 = 5$. It can be noticed that for this value of λ_1, the observer dynamics is faster than the PMSM currents dynamics.

2) Parameters k_i, k_p: In order to get the maximum amplification of the fault frequencies components, it is not necessarily appropriate to adjust the filter on the first fault frequency f_d, ignoring the other components ($n \cdot f_d$ with $n = 2, 3, ...$). To overcome this problem, the transfer function magnitude ($|F_{34}(n \cdot f_d)|$) is calculated for the first four fault frequencies as

$$G = |F_{34}(f_d)| + |F_{34}(2f_d)| + |F_{34}(3f_d)| + |F_{34}(4f_d)|.$$

(20)

Fig. 7 shows the evolution of the sum G for a fault frequency of 22 Hz in function of the two parameters k_i and k_p. It can be clearly seen on this figure that four maxima corresponding to $f_d, 2f_d, 3f_d$, and $4f_d$ exist.

From this figure, it can be deduced that several maxima can be chosen to amplify the fault frequencies. The optimal value of k_p is kept constant and equal to $k_p = -0.04$. The corresponding values of k_i are respectively equal to 16, 80, 188, and 340 so as to coincide with the first four fault frequencies $f_d = 22, 2f_d = 44, 3f_d = 66$, and $4f_d = 88$ Hz. In order to validate the obtained results, different tests are performed on MATLAB/Simulink environment.
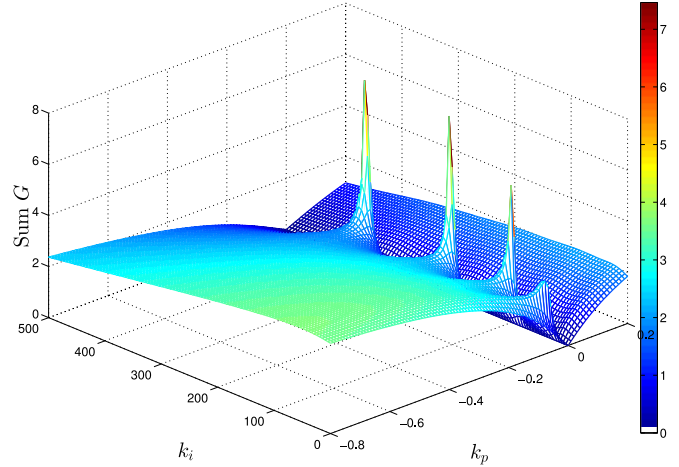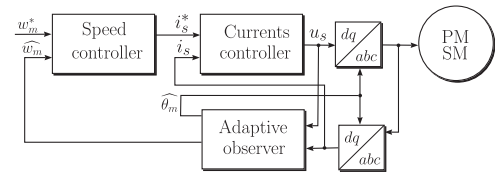

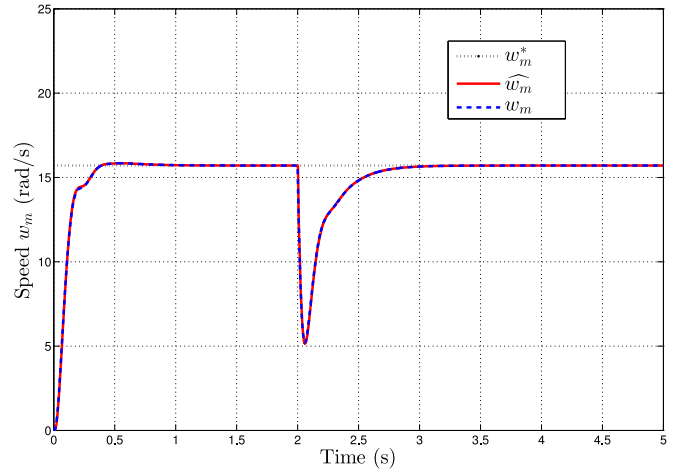Fig. 8. Block diagram of the PMSM sensorless vector control.

Fig. 9. Simulation results of the adaptive observer.

C. Simulation Results

The block diagram of the PMSM sensorless vector control is shown in Fig. 8. PI controllers are used for the currents and speed loop, respectively. The reference current i_d is imposed to 0. The PMSM parameters are given in Appendix A. In order to analyze the observer described above, a simulation at an operating point (20% of the nominal speed which corresponds to $f_m = 2.5$ Hz and 100% load torque) is studied. Fig. 9 illustrates the estimated, the measured, and the reference speed signals, respectively, $\widehat{w}_m$, w_m, and w_m^*. We can notice that the estimated speed is able to track the measured one.
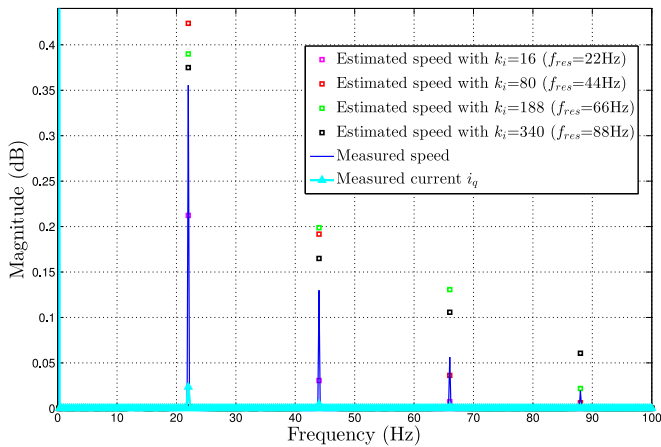
Fig. 10.   Influence of the parameter k_i on the speed spectrum with the parameters $k_p = -0.04$ and $\lambda_1 = 5$.
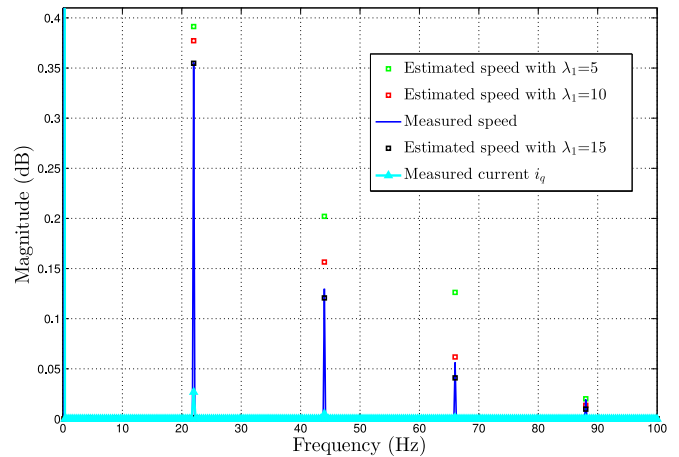

Fig. 11.   Influence of the parameter k_p on the speed spectrum with the parameters $k_i = 188$ and $\lambda_1 = 5$.

Fig. 12.   Influence of the parameter λ_1 on the speed spectrum with the parameters $k_p = -0.04$ and $k_i = 188$.
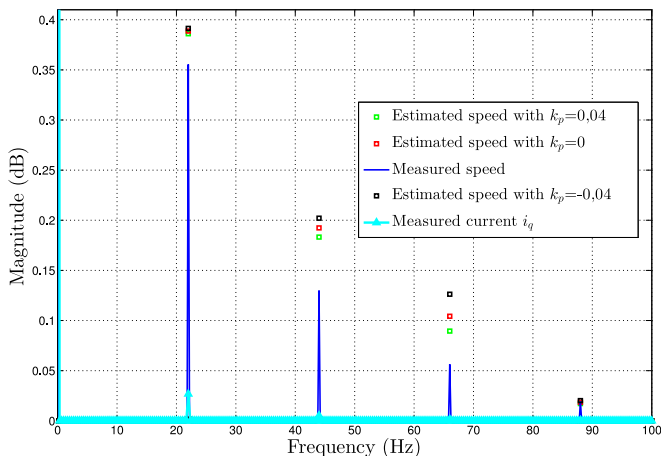

Fig. 13.   Experimental setup.

A localized fault with nine impacts for one rotor revolution ($f_d = 22$ Hz) is introduced in the system by means of the load torque. Signals are filtered using a classical synchronous averaging in order to only conserve components related to fault frequencies. Figs. 10, 11, and 12 show the rotation speed spectrum for different values of the parameters k_i, k_p, and λ_1. Note that the current i_q has been added to confirm that the speed is a better candidate for fault detection.

Fig. 10 shows the evolution of the estimated speed spectrum when the parameter k_i is varying, which means that the filter resonance frequency is changing. It is clear that the first fault at $k_i = 16$ does not give any good results because of the integral effect (with a very low integration gain, the estimated speed dynamics is too slow). It can be seen that the estimated speed contains more important fault harmonics than the measured one. Moreover, the resonance frequency at 45 Hz (for $k_i = 80$) gives a significant fault signatures for the first and second fault frequency (f_d, $2f_d$). Regarding the third and the fourth fault components, the magnitudes of the faults harmonics are lower compared to other values of k_i. The best results are obtained for $k_i = 188$, which corresponds to a resonance

frequency of 66 Hz. This choice corresponds to $3f_d$ which represents the third maximum (see Fig. 10).

Fig. 11 shows that for $k_p = -0.04$ (the value corresponding to the maxima obtained before) the fault frequency components are amplified on the estimated speed. Fig. 12 shows that for $\lambda_1 = 5$, the fault amplitude increases. However, if the value of λ_1 increases to ($\lambda_1 = 15$), the fault amplitude decreases. It can be explained by the fact that with a high value of λ_1, the filter becomes more selective (the Q factor becomes lower), which leads to a decrease of the fault amplitude.

V. EXPERIMENTAL RESULTS

A. Test Bench Description

Fig. 13 illustrates the complete experimental setup which includes two PMSMs. The synchronous motor (PMSM) is driven by a variable-speed drive (VSD). The rotor position (measured by an incremental encoder) is returned directly to the VSD.

The permanent magnet synchronous generator is connected to a passive load. The signals recording is performed by a dSPACE-DS1104 card and the acquisition is made in MATLAB environment.

The localized fault is emulated using an original mechanical system designed in our laboratory. The emulator (see Fig. 14) is mounted on the coupling motor/generator. It consists of a

Fig. 14.   Localized fault emulator.

TABLE II
FAULT SIGNATURES MAGNITUDES ON THE ESTIMATED SPEED SIGNAL $\widehat{w}$

		Magnitude (dB)				
		f_d	$2f_d$	$3f_d$	$4f_d$	$\sum$
Speed estimation parameters	max_1	0.1676	0.042	0.0228	0.02	0.2524
	max_2	**0.3744**	0.3083	0.103	0.002	0.8057
	max_3	0.3142	**0.3192**	**0.3967**	0.0817	0.12
	max_4	0.2897	0.2468	0.3183	**0.2535**	0.13

roller mounted vertically over a nine teeth sprocket. This system emulates a fault occurring nine times per turn. Therefore, the obtained fault frequency f_d is the number of impacts times the fundamental frequency of rotor rotation $f_d = 9 \cdot f_m$. A spring is mounted above the roller to adjust the force in order to get different fault severities.

B. Fault Amplification Results

Experimental tests are performed for 20% of the nominal speed ($150\,\mathrm{r/min}$). In this case, the fault frequency corresponds to $f_d = 2.5 \times 9 = 22.5\,\mathrm{Hz}$. The variables in the $\{d/q\}$ frame are calculated from the measures given by the current and voltage sensors and the position measure provided by the incremental encoder. The observer gains are set for the four maxima shown in Fig. 7 as follows:

1) max_1: $k_i = 16$, $k_p = -0.04$ and $\lambda_1 = 5$;
2) max_2: $k_i = 80$, $k_p = -0.04$ and $\lambda_1 = 5$;
3) max_3: $k_i = 188$, $k_p = -0.04$ and $\lambda_1 = 5$;
4) max_4: $k_i = 340$, $k_p = -0.04$ and $\lambda_1 = 5$.

Fig. 15 shows the spectrum of the current i_q with and without fault and the estimated speed $\widehat{w}$ for the four maxima. Table II shows the fault magnitude sum (noted in the table by the symbol $\sum$).
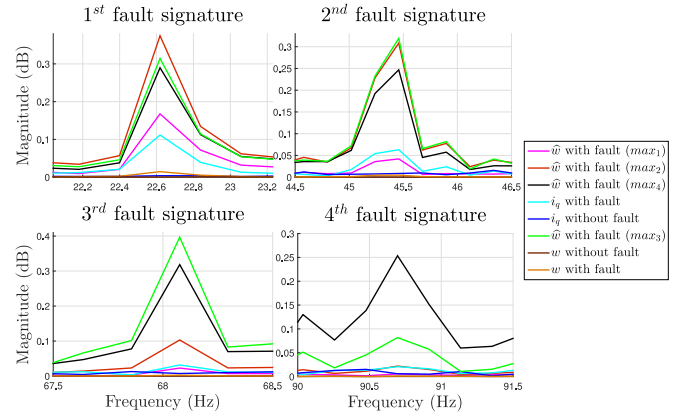

Fig. 15.   Zoom on the first four faults signatures f_d, $2f_d$, $3f_d$, and $4f_d$ for the current i_q, measured speed w with and without fault and the estimated speed $\widehat{w}$ with fault.

It can be noticed in this figure that the fault amplitude is actually improved in the four cases and especially for max_3 and max_4, which give the highest magnitude sums $\sum$ (see Table II). These results validate the fault signatures amplification and improve the detection of localized mechanical faults.

C. Fault Detection Technique

In order to detect the localized mechanical fault produced by the developed test bench, a simple technique called time synchronous averaging (TSA), which is known for bearing failure detection in electrical machines [22], was used.

By synchronizing a trigger signal with the fault frequency, the TSA just extracts the fault frequencies from the signal and delete all the undesired components. But first of all the fault frequency has to be determined precisely. To this end, an estimation technique based on a nonlinear programming is chosen (Levenberg Marquardt algorithm). This technique is detailed in [23].

After the fault frequency estimation, TSA generates a signal which just contains the fault frequencies. To validate the efficiency of the localized mechanical fault detection procedure presented in this paper, a fault indicator ind is calculated for the first four fault frequencies:

$$\mathrm{ind} = \sum_{n=1}^{4} Y(n \cdot f_d) \qquad (21)$$

where

$Y(f)$ signal generated by TSA;
f_d fault frequency;
n fault frequency multiples (here, only the first four fault frequencies are considered).

A second indicator R is defined: it represents the ratio between ind before and after the fault

$$R = \frac{\mathrm{ind}_f}{\mathrm{ind}_h} \qquad (22)$$

where ind_f is the indicator ind calculated for a faulty case, and

<div style="display:flex">
<div>

TABLE III
CALCULATION RESULTS OF THE INDICATOR R

Tests	Rotation speed 20% of the nominal speed					
	1	2	3	4	5	$\bar{R}$
i_q	8.3103	7.9331	6.4306	5.4439	7.0754	**7.0387**
$\max_1$	9.2212	5.4750	6.9620	8.7500	8.6333	**7.8083**
$\max_2$	8.8656	10.2680	7.0577	6.8873	7.7747	**8.1707**
$\max_3$	9.2972	8.8485	6.3531	8.9750	7.9876	**8.2923**
$\max_4$	10.5888	8.1761	8.1818	6.7293	9.2616	**8.5875**

</div>
<div>

TABLE IV
PARAMETERS OF THE MOTOR LSRPM 160MP

Nominal power	7.8 kW
Nominal voltage	360 V
Nominal current	15 A
Nominal speed	750 r/ min
Nominal frequency	50 Hz
Stator resistance R_s	1 Ω
Direct-axis inductance L_d	25.7 mH
Quadrature-axis inductance L_q	25.9 mH
Permanent magnet flux ψ_{pm}	0.8 Wb
Inertia	0.0418 Kg.m²

</div>
</div>

ind_h is the indicator ind calculated for a healthy case (using the same parameters used in the faulty one).

Table III represents the results obtained using the procedure cited in [23] and applied to the measured current i_q and the different estimated speeds by the observer adjusted for the four maxima presented before. A set of five tests has been realized to illustrate the efficiency of the proposed fault detection procedure and fault indicator. In this table, it can be seen that the mean value of R ($\bar{R}$) is more important in the four cases for the estimated speed by the observer compared to the measured current i_q.

VI. CONCLUSION

This paper is dedicated to the study of the observer in $\{d/q\}$. Initially, the observer model was linearized to examine the transfer functions between the estimated state variables and the inputs (measured variables). It has been shown that the parameters k_i, k_p, and λ_1 influence the fault frequency amplitude. The parameter k_i affects the resonance frequency which can be chosen as one of the default frequencies $n \cdot f_d$. The parameter k_p has an impact on the Q factor as well as the static gain. The parameter λ_1 influences only the Q factor. The following strategy is proposed to make a judicious choice of these three observer gains.

1) λ_1 is chosen to ensure a faster observer dynamics than the current loop one.
2) k_i is chosen to coincide with a fault frequency.
3) k_p is chosen so that the sum G corresponds to a maximum.

An original test bench was proposed to emulate the localized mechanical faults. The simulation and experimental results confirmed the proposed diagnosis strategy. The fault indicator $\bar{R}$ is improved with the estimated speed compared to the measured current i_q. It can be deduced that the observer output is much richer in terms of fault frequencies amplitude than the input of the observer.

In control of electrical machines, observers are widely used to limit the speed sensors requirements (sensorless control). The novelty of this paper is that a speed observer is designed and its gains are adjusted to amplify the localized mechanical fault signatures.

The observer gains are just settled here in terms of fault amplification. In the future, this study has to be extended to dynamics and stability analysis of the observer. Further investigations are necessary to determine a compromise to satisfy convergence and fault detection requirements.

APPENDIX A

The Leroy-Somer Motor characteristics and parameters (LSRPM 160 MP) are presented in Table IV.

APPENDIX B

$$
\begin{cases}
a_1 = k_i \cdot iq_0 - k_p \left[iq_0.\lambda_1 - id_0.\lambda_2 - \frac{L_d.id_0.w_0}{L_q} \right. \\
\qquad \left. - \frac{L_d.\psi_{pm}.w_0}{L_q^2} - \lambda_2 \frac{\psi_{pm}}{L_q} + \frac{R_s.iq_0}{L_d} \right] \\
a_2 = -k_i \left(\frac{\psi_{pm}}{L_q} + id_0 \right) - k_p \left[-id_0.\lambda_1 - iq_0.\lambda_2 \right. \\
\qquad \left. - \frac{R_s.id_0}{L_q} - \lambda_1 \frac{\psi_{pm}}{L_q} - \frac{R_s.\psi_{pm}}{L_q^2} - \frac{L_q.w_0.iq_0}{L_d} \right] \\
a_3 = -k_p \left[-\frac{\psi_{pm}^2}{L_q^2} - \frac{L_d.\psi_{pm}.id_0}{L_q^2} - \frac{id_0.\psi_{pm}}{L_q} \right. \\
\qquad \left. - id_0^2 \frac{L_d}{L_q} - iq_0^2 \frac{L_q}{L_d} \right]
\end{cases}
$$

$$
\begin{cases}
b_3 = L_d^2 L_q^3 \\
b_2 = L_d L_q (k_p L_d^2 L_q id_0^2 + k_p L_d^2 id_0 \phi_f + 2\lambda_1 L_d L_q^2 \\
\qquad + k_p L_d L_q id_0 \phi_f + R_s L_d L_q + k_p L_d \phi_f^2 + k_p L_q^3 iq_0^2 \\
\qquad + R_s L_q^2) \\
b_1 = L_d L_q (k_p L_d^2 L_q id0^2 \lambda_1 + k_i L_d^2 L_q id_0^2 \\
\qquad - k_p L_d^2 L_q id_0 iq_0 \lambda_2 \\
\qquad + L_d^2 L_q \lambda_2 w_0 + k_p L_d^2 id_0 \lambda_1 \phi_f + k_i L_d^2 id_0 \phi_f \\
\qquad + L_d L_q^2 \lambda_1^2 \\
\qquad + L d L q^2 \lambda_2^2 + L_d L_q^2 w_0^2 + k_p L_d L_q R_s id_0^2 \\
\qquad + L_d L_q R_s \lambda_1 \\
\qquad + k_p L_d L_q id_0 \lambda_1 \phi_f + k_i L_d L_q id_0 \phi_f \\
\qquad - k_p L_d L_q iq_0 \lambda_2 \phi_f \\
\qquad + k_p L_d L_q iq_0 \phi_f w_0 + k_p L_d R_s id_0 \phi_f + k_p L_d \lambda_1 \phi_f^2 \\
\qquad + k_i L_d \phi_f^2 + k_p L_q^3 id_0 iq_0 \lambda_2 + k_p L_q^3 iq_0^2 \lambda_1 + k_i L_q^3 iq_0^2 \\
\qquad + L_q^3 \lambda_2 w_0 + k_p L_q^2 R_s iq_0^2 + L_q^2 R_s \lambda_1 \\
\qquad + k_p L_q^2 iq_0 \lambda2 \phi_f \\
\qquad - k_p L_q^2 iq_0 \phi_f w_0 + L_q R_s^2 + k p L_q R_s id_0 \phi_f \\
\qquad + k_p R_s \phi_f^2) \\
b_0 = L_d L_q (R_s k_i \phi_f^2 + L_d k_i \lambda_1 \phi_f^2 + L_q^2 R_s iq_0^2 k_i \\
\qquad + L_q^3 iq_0^2 k_i \lambda_1 \\
\qquad + L_d R_s id_0 k_i \phi_f + L_q R_s id_0 k_i \phi_f + L_d L_q R_s id_0^2 k_i \\
\qquad + L_q^3 id_0 iq_0 k_i \lambda_2 + L_q^2 id_0 k_i \lambda_1 \phi_f + L_q^2 iq_0 k_i \lambda_2 \phi_f \\
\qquad - L_q^2 iq_0 k_i \phi_f w_0 + L_d^2 L_q id_0^2 k_i \lambda_1 - L_d^2 L_q id_0 iq_0 k_i \lambda_2 \\
\qquad + L_d L_q id_0 k_i \lambda_1 \phi_f - L_d L_q iq_0 k_i \lambda_2 \phi_f \\
\qquad + L_d L_q iq_0 k_i \phi_f w_0).
\end{cases}
$$

REFERENCES

[1] A. H. Bonnett and C. Yung, "Increased efficiency versus increased reliability," *IEEE Ind. Appl. Mag.*, vol. 14, no. 1, pp. 29–36, Jan. 2008.

[2] X. Jin, M. Zhao, T. W. S. Chow, and M. Pecht, "Motor bearing fault diagnosis using trace ratio linear discriminant analysis," *IEEE Trans. Ind. Electron.*, vol. 61, no. 5, pp. 2441–2451, May 2014.

[3] M. Riera-Guasp, J. A. Antonino-Daviu, and G. Capolino, "Advances in electrical machine, power electronic, and drive condition monitoring and fault detection: State of the art," *IEEE Trans. Ind. Electron.*, vol. 62, no. 3, pp. 1746–1759, Dec. 2014.

[4] W. Qiao and D. Lu, "A survey on wind turbine condition monitoring and fault diagnosis—Part II: Signals and signal processing methods," *IEEE Trans. Ind. Electron.*, vol. 62, no. 10, pp. 6546–6557, Apr. 2015.

[5] E. H. El Bouchikhi, V. Choqueuse, and M. Benbouzid, "Induction machine faults detection using stator current parametric spectral estimation," *Mech. Syst. Signal Process.*, vol. 52–53, pp. 447–464, Feb. 2015.

[6] M. Seera, C. P. Lim, D. Ishak, and H. Singh, "Fault detection and diagnosis of induction motors using motor current signature analysis and a hybrid FMM-cart model," *IEEE Trans. Neural Netw.*, vol. 23, no. 4, pp. 97–108, Jan. 2012.

[7] X. Gong and W. Qiao, "Imbalance fault detection of direct-drive wind turbines using generator current signals," *IEEE Trans. Energy Convers.*, vol. 27, no. 2, pp. 468–476, Jun. 2012.

[8] T. Gerber, N. Martin, and C. Mailhes, "Time-frequency tracking of spectral structures estimated by a data-driven method," *IEEE Trans. Ind. Electron.*, vol. 62, no. 10, pp. 6616–6626, Jul. 2015.

[9] W. Zhou, T. Habetler, and R. Harley, "Stator current-based bearing fault detection techniques: A general review," in *Proc. IEEE Int. Symp. Diagnostics Elect. Mach. Power Electron. Drives*, Cracow, Poland, Sep. 2007, pp. 7–10.

[10] E. C. C. Lau and H. W. Ngan, "Detection of motor bearing outer raceway defect by wavelet packet transformed motor current signature analysis," *IEEE Trans. Instrum. Meas.*, vol. 59, no. 10, pp. 2683–2690, Oct. 2010.

[11] V. F. Pires, M. Kadivonga, J. F. Martins, and A. J. Pires, "Motor square current signature analysis for induction motor rotor diagnosis," *Measurement*, vol. 46, pp. 942–948, Feb. 2013.

[12] H. Henao, G.-A. Capolino, and M. Fernandez-Cabanas, "Trends in fault diagnosis for electrical machines," *IEEE Ind. Electron. Mag.*, vol. 8, no. 2, pp. 31–42, Jun. 2014.

[13] F. Immovilli, A. Bellini, R. Rubini, and C. Tassoni, "Diagnosis of bearing faults in induction machines by vibration or current signals: A critical comparison," *IEEE Trans. Ind. Appl.*, vol. 46, no. 4, pp. 1350–1359, Jul./Aug. 2010.

[14] J. Lee, J. Hong, K. Nam, and R. Ortega, "Sensorless control of surface-mount permanent-magnet synchronous motors based on a nonlinear observer," *IEEE Trans. Power Electron.*, vol. 25, no. 2, pp. 290–297, Feb. 2010.

[15] B. Trajin, J. Regnier, and J. Faucher, "Detection of bearing faults in asynchronous motors using Luenberger speed observer," in *Proc. 34th Annu. Conf. IEEE Ind. Electron. Soc.*, Orlando, FL, USA, Nov. 2008, pp. 3073–3078.

[16] B. Trajin, and J. Regnierand, J. Faucher, "Comparison between stator current and estimated mechanical speed for the detection of bearing wear in asynchronous drives," *IEEE Trans. Ind. Electron.*, vol. 56, no. 11, pp. 4700–4709, Oct. 2009.

[17] M. Pineda-Sanchez, M. Riera-Guasp, J. Pons-Llinares, V. Climente-Alarcon, and J. Perez-Cruz, "Diagnosis of induction machines under transient conditions through the Instantaneous Frequency of the fault components," *Proc. 19th Int. Conf. Elect. Mach.*, Rome, Italy, Sep. 2010, pp. 1–6.

[18] M. Hamadache, D. Lee, and K. C. Veluvolu, "Rotor speed-based bearing fault diagnosis (RSB-BFD) under variable speed and constant load," *IEEE Trans. Ind. Electron.*, vol. 62, no. 10, pp. 6486–6494, Mar. 2015.

[19] H. Luo, Q. Yin, X. Li, and Y. Liu, "An improved adaptive observer for permanent magnet synchronous motor," in *Proc. 9th IEEE Conf. Ind. Electron. Appl.*, Hangzhou, China, Jun. 2014, pp. 1301–1306.

[20] A. Piippo, M. Hinkkanen, and J. Luomi, "Analysis of an adaptive observer for sensorless control of interior permanent magnet synchronous motors," *IEEE Trans. Ind. Electron.*, vol. 55, no. 3, pp. 570–576, Feb. 2008.

[21] E. Etien, C. Chaigne, and N. Bensiali, "On the stability of full adaptive observer for induction motor in regenerating mode," *IEEE Trans. Ind. Electron.*, vol. 57, no. 5, pp. 1599–1608, May 2010.

[22] P. D. McFadden and M. M. Toozhz, "Application of synchronous averaging to vibration monitoring of rolling element bearings," *Mech. Syst. Signal Process.*, vol. 14, no. 6, pp. 891–906, Nov. 2000.

[23] M. L. Masmoudi, E. Etien, S. Moreau, and A. Sakout, "Bearing fault diagnosis using a pre-filtering and a spectral identification algorithm," in *Proc. 39th Annu. Conf. IEEE Ind. Electron. Soc.,*, Vienna, Austria, Nov. 2013, pp. 5476–5481.
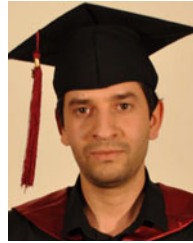
Mohamed Lamine Masmoudi was born in Batna, Algeria, in 1986. He received the B.Sc. degree in electrical engineering from the University of Batna, Batna, Algeria, in 2010, the M.Sc. degree in automatic control from the University of Poitiers, Poitiers, France, in 2011, and the Ph.D. degree in electrical and computer engineering from the University of La Rochelle, La Rochelle, France, in 2015.

He is currently a Research and Development Electrical Engineer at the SATT Grand Centre, Poitiers, France. His research interests include electrical drives, fault diagnosis and controller design.

Erik Etien was born in France in 1970. He received the Ph.D. degree in automatic control from the University of Poitiers, Poitiers, France, in 1999.

He is currently an Associate Professor with HDR at the University of Poitiers. His research interests include the development of soft sensors in the field of electrical engineering.

Sandrine Moreau was born in France in 1972. She received the Ph.D. degree in automatic control from the University of Poitiers, Poitiers, France, in 1999.

She is currently an Assistant Professor at the University of Poitiers. Her major research interests include modeling, identification, control, and diagnosis of electrical machines associated with static converters for different applications (renewable energies, robotics, etc.).

Anas Sakout was born in Morocco in 1963. He received the Ph.D. degree in mechanical engineering from the University of Le Havre, Le Havre, France, in 1994.

He is currently a Professor at the University of La Rochelle, La Rochelle, France. His research interests focus on mechanics and physics, in particular, aeroacoustics, fluid structure interaction, fluid dynamics, room acoustics, and perception.